Recent Seismic Studies at the East Pacific Rise 8°20'–10°10'N and Endeavour Segment

Insights into Mid-Ocean Ridge Hydrothermal and Magmatic Processes

BY SUZANNE M. CARBOTTE, JUAN PABLO CANALES,
MLADEN R. NEDIMOVIĆ, HÉLÈNE CARTON, AND JOHN C. MUTTER

R/V Marcus Langseth. Courtesy of Sandbox Studios, San Francisco, with permission from Lamont-Doherty Earth Observatory Office of Marine Operations

ABSTRACT. As part of the suite of multidisciplinary investigations undertaken by the Ridge 2000 Program, new multichannel seismic studies of crustal structure were conducted at the East Pacific Rise (EPR) 8°20'–10°10'N and Endeavour Segment of the Juan de Fuca Ridge. These studies provide important insights into magmatic systems and hydrothermal flow in these regions, with broader implications for fast- and intermediate-spreading mid-ocean ridges. A mid-crust magma body is imaged beneath Endeavour Segment underlying all known vent fields, suggesting that prior notions of a tectonically driven hydrothermal system at this site can be ruled out. There is evidence at both sites that the axial magma body is segmented on a similar 5–20 km length scale, with implications for the geometry of high-temperature axial hydrothermal flow and for lava geochemistry. The new data provide the first seismic reflection images of magma sills in the crust away from the axial melt lens. These off-axis magma reservoirs are the likely source of more-evolved lavas typically sampled on the ridge flanks and may be associated with off-axis hydrothermal venting, which has recently been discovered within the EPR site. Clusters of seismic reflection events at the base of the crust are observed, and localized regions of thick Moho Transition Zone, with frozen or partially molten gabbro lenses embedded within mantle rocks, are inferred. Studies of the upper crust on the flanks of Endeavour Segment provide new insights into the low-temperature hydrothermal flow that continues long after crustal formation. Precipitation of alteration minerals due to fluid flow leads to changes in P-wave velocities within seismic Layer 2A (the uppermost layer of the oceanic crust) that vary markedly with extent of sediment blanketing the crust. In addition, intermediate-scale variations in the structure of Layers 2A and 2B with local topography are observed that may result from topographically driven fluid upflow and downflow on the ridge flanks.

INTRODUCTION

The Endeavour Segment of the Juan de Fuca Ridge (JdFR) and the East Pacific Rise (EPR) from 8°–11°N were selected for focused investigations under the Ridge 2000 Program as contrasting intermediate-spreading tectonic (Endeavour) and fast-spreading magmatic (EPR) ridge systems (see Kelley et al., 2012, and Fornari et al., 2012, both in this issue). From the early near-bottom observations of Kappel and Ryan (1986), Endeavour Segment was interpreted to be in the tectonic phase of an episodic magmatic-tectonic cycle.

Hydrothermal circulation fueled by heat extracted from cracking and cooling of the lower crust in the absence of magma was invoked to explain the robust and long-lived Endeavour hydrothermal vent fields (Wilcock and Delaney, 1996). In contrast, the EPR was believed to be a fundamentally different, magmatically driven system with hydrothermal circulation closely coupled to dike intrusion from a steady-state magma lens in the mid-crust (e.g., Haymon et al., 1991).

These inferences were based, in large part, on evidence from early seismic studies of crustal structure conducted at both sites in the 1980s. Multichannel seismic (MCS) reflection data acquired in 1985 with R/V *Conrad* revealed a bright reflection in the mid-crust beneath the EPR, attributed to a thin layer of melt above a broader zone of low seismic velocities in the lower crust (Detrick et al., 1987; Vera et al., 1990; Kent et al., 1993a,b). In contrast, significant low-velocity anomalies in the crust indicative of a magma body were not found under the axis at Endeavour Segment (Cudrak and Clowes, 1993; White and Clowes, 1994). While a faint reflector was imaged in the mid-crust beneath the axis in an MCS study of Endeavour in 1985, it was attributed to an increase in seismic velocity related to a hydrothermal boundary and not the presence of melt (Rohr et al., 1988; White and Clowes, 1994).

As part of the suite of multidisciplinary investigations of ocean crustal formation and hydrothermal processes undertaken by the Ridge 2000 Program, new seismic studies of crustal structure employing modern MCS techniques were conducted at both the EPR and Endeavour Integrated Study Sites (ISSs). During seafloor spreading, mass and heat fluxes from the deep Earth are converted into new crust through magmatic processes that drive hydrothermal fluid circulation, which in turn cools the crust and alters its composition. MCS techniques are well suited for studying these processes. They provide detailed images of boundaries between layers with significant contrasts in physical properties and enable high-resolution velocity models to be constructed for

the shallow crust using refracted seismic arrivals recorded with the long-offset streamers used in modern surveys. From the new MCS studies at Endeavour and EPR ISSs, constraints on the geometry, depth, and dimensions of the mid-crust magma lens now known to be present at both sites have been obtained, as well as properties of the upper crust above the magma body (seismic Layers 2A and 2B) through which axial hydrothermal fluid circulation occurs. The Moho reflection at the base of the crust is well imaged, along with other unexpected reflectivity within the crust and below, providing new insights into spatial variations in magma production and delivery at these spreading centers.

At Endeavour, new MCS data were acquired in 2002 as part of a comprehensive regional investigation of the JdFR that included focused surveys of the axial region of all ridge segments, as well as three 300 km long transects on the ridge flanks for studies of crustal evolution (Canales et al., 2005, 2006, 2009; Carbotte et al., 2006, 2008; Nedimović et al., 2005, 2008; Van Ark et al., 2007; Newman et al., 2011). At the EPR, new data were acquired in 2008 as part of the first academic multisource and multistreamer three-dimensional (3D) MCS study ever conducted (Mutter et al., 2009; Canales et al., in press). Here, we review the major findings arising from these studies regarding axial and ridge flank processes. The new observations reveal fundamental similarities in axial processes at the two sites and changes in upper crustal structure that can be linked to hydrothermal flow both on axis and on the ridge flanks. While our focus here is on the recent MCS studies conducted as part of Ridge 2000, these

studies complement and build upon a wealth of knowledge of crustal and upper mantle structure, primarily from the EPR site, derived from the earlier MCS investigations (Detrick et al., 1987; Vera et al., 1990; Kent et al., 1993a,b, 2000; Harding et al., 1993; Singh et al., 2006) and geophysical studies using other techniques (e.g., Crawford et al., 1999, 2002; Dunn et al., 1997, 2000; Toomey et al., 2007). New studies employing these techniques are underway at the Endeavour and EPR sites (Key and Constable, 2005; Toomey et al., 2010; Zha et al., 2010), and exciting new results are anticipated in the coming years.

NEW FINDINGS
Axial Magma Reservoirs at Endeavour and EPR ISSs
Endeavour Segment
Although a significant crustal magma body was not detected in the early seismic studies of Endeavour (Cudrak and Clowes, 1993; White and Clowes, 1994), the new data reveal a bright reflection beneath the central ~ 20 km of the 90 km long segment (Van Ark et al., 2007; Figures 1A and 2). This axial reflection is identified as a reversed polarity event on common mid-point gathers, indicating it arises from a decrease in seismic velocity consistent

with the presence of melt. Estimates of melt content within the magma lens derived from waveform studies of the axial magma chamber (AMC) reflection (e.g., Collier and Singh, 1997) have not been possible to obtain due to poor signal quality at far source-receiver offsets, likely due to rough seafloor topography. The depth of the magma lens reflection, often referred to as the AMC reflection, varies by over 1 km, from 2.2 to 3.3 km, and is shallowest beneath the central portion of the axial ridge (Van Ark et al., 2007). This central portion of the segment coincides with the on-axis projection of the Heckle seamount chain, and the presence of the local mantle melt anomaly associated with these volcanoes may contribute to the focusing of mantle melt delivery within Endeavour Segment (Carbotte et al., 2008).

Using variations in the amplitude and depth of the AMC reflection, Van Ark et al. (2007) infer that the magma body beneath Endeavour is composed of four segments with boundaries at ~ 47°54.7'N, 47°56.8'N, and 48°00.5'N (Figures 1A and 2). A crustal magma body underlies all of the major active high-temperature vent fields at Endeavour. High Rise, Salty Dawg, and Sasquatch overlie the shallowest lens

Suzanne M. Carbotte (carbotte@ldeo.columbia.edu) is Bruce C. Heezen/Lamont Research Professor, Lamont-Doherty Earth Observatory, Columbia University, Palisades, NY, USA. **Juan Pablo Canales** is Associate Scientist with Tenure, Geology and Geophysics Department, Woods Hole Oceanographic Institution, Woods Hole, MA, USA. **Mladen R. Nedimović** is Canada Research Chair in Geophysics and Petroleum Exploration, and Associate Professor, Dalhousie University, Halifax, Canada, and Adjunct Research Scientist, Lamont-Doherty Earth Observatory, Columbia University, Palisades, NY, USA. **Hélène Carton** is Lamont Assistant Research Professor, Lamont-Doherty Earth Observatory, Columbia University, Palisades, NY, USA. **John C. Mutter** is Professor of Earth and Environmental Sciences, Columbia University, Palisades, NY, USA.

segment from 47°56.8'N and 48°00.5'N. The Main Endeavour vent field is located within a zone of complex reflectivity at the southern end of this segment, and the deeper lens segment to the south underlies Mothra. While it is likely that segmentation of the magma lens plays an important role in the patterns of venting along the ridge, the existing 2D seismic data are insufficient to resolve detailed geometry and distribution of melt at length scales appropriate for linking with seafloor structures, and future 3D seismic studies will be needed.

Another new insight from the 2002 reflection survey concerns the origin of the shallowly rifted axial high topography along the JdFR, which had been attributed to tectonic extension during amagmatic phases (Kappel and Ryan, 1986), analogous to the formation of rift valleys at slow-spreading ridges. The magma lens reflection at Endeavour is narrowly focused beneath the 25 km long shallowly rifted axial volcanic ridge where there is a prominent 0.8–1.4 km wide axial graben (Glickson et al., 2007). The presence of a well-defined symmetric axial graben at the seafloor, where a magma lens is observed in the subsurface, is found at all JdFR segments, and this graben appears to be a magmatic rather than a tectonically generated structure, linked to dike intrusion and magma withdrawal from the magma lens (Carbotte et al., 2006). If the axial graben were generated by amagmatic extension, as previously assumed, deep wide grabens would be expected where the magma body is absent and where ongoing plate separation should be accommodated by tectonic extension. Instead, the opposite relationship is observed; rift topography diminishes

where the magma lens is absent, and the deepest grabens are found where the magma lens is shallowest. As a magmatically generated depression linked to the presence of a crustal magma body, the axial graben found along the JdFR is similar to the axial summit trough (AST) at the EPR (Fornari et al., 1998), although much larger in scale.

East Pacific Rise 8°20'–10°10'N

The overall geometry and dimensions of the mid-crust magma sill within the EPR site were established from the pioneering 1985 MCS experiment within the region (e.g., Detrick et al., 1987; Vera et al., 1990; Kent et al., 1993a,b). This experiment revealed an axial magma body that is only a few tens of meters
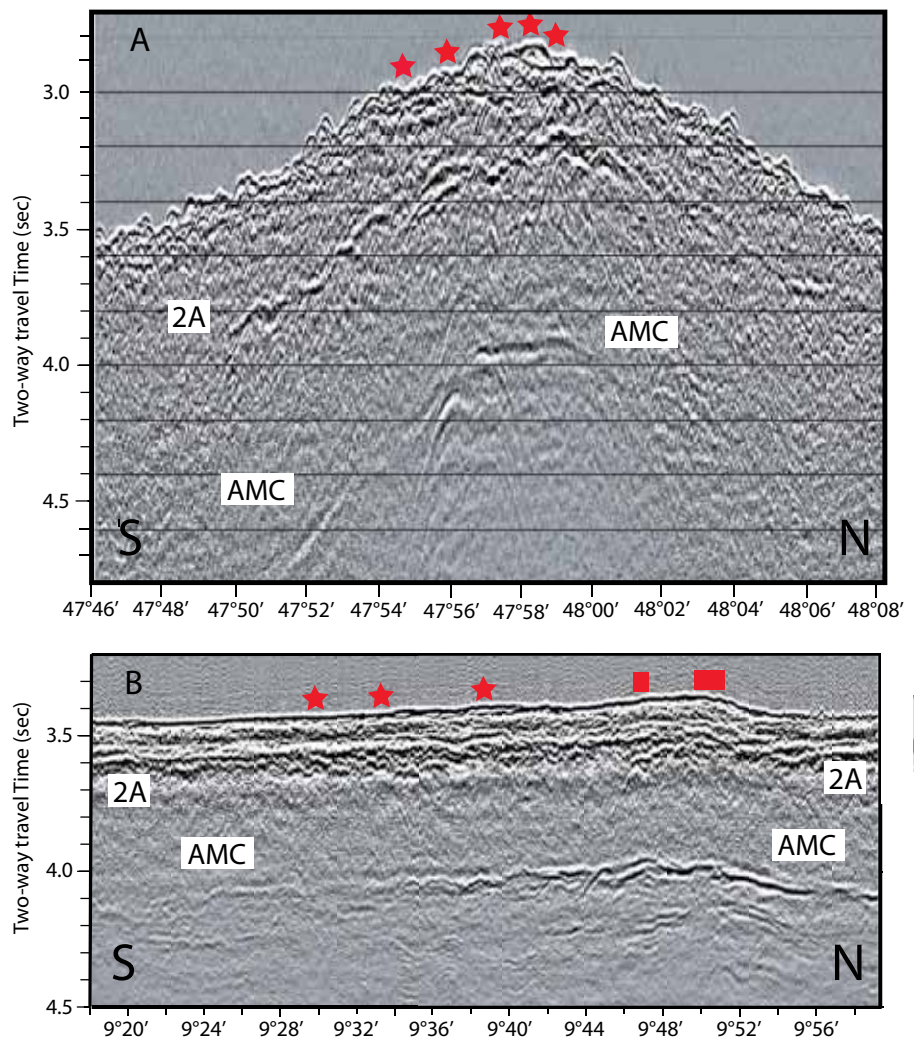

Figure 1. Seismic profiles showing the magma lens reflection detected along the axis of the (A) Endeavour and (B) East Pacific Rise (EPR). (A) Along-axis line 14 from the Endeavour multichannel seismic survey showing the axial magma chamber (AMC) and seismic Layer 2A events from Van Ark et al. (2007). Red stars show locations of the five large hydrothermal vent fields (from south to north: Mothra, Main Endeavour, High Rise, Salty Dawg, Sasquatch; see Figure 2 for location). (B) Along-axis line axis2r1 from the EPR 2008 multichannel seismic survey showing the AMC and seismic Layer 2A events. Red stars indicate active high-temperature hydrothermal vents (from south to north: K, D, B). Red bars indicate closely spaced vents at 9°46'N (L, A, V) and 9°51'N (TWP, BM41, P, Bio 9, Biovent).

thick, variable in width (< 0.5 to 4.5 km), and disrupted at a number of small ridge axis tectonic discontinuities. The data collected in 2008 extend the earlier observations and support investigations of the fine-scale structure of the magma body and relationships with hydrothermal venting and recently erupted lavas at the overlying seafloor.

In contrast to Endeavour Segment, the magma body is detected beneath most (~ 85%) of the first-order EPR segment between the Clipperton and Siqueiros Transform Faults. The AMC lies at average depths of 1.6 km, ~ 1 km shallower than at Endeavour, and the thinner crustal lid above the AMC at the EPR must play an important role in accounting for the observed differences in axial faulting and hydrothermal processes at these ridge crests. The recently acquired 3D MCS data set reveals that the axial magma body is segmented on a finer scale than previously appreciated, with disruptions in the imaged magma lens reflection and complex zones of overlap, and offset of melt zones that define four segments within the region of 3D coverage from 9°42'N to 9°57'N (Carton et al., 2010). Beyond the zone of 3D coverage, axially centered seismic lines acquired for the length of the EPR between 8°20'N and 10°10'N reveal numerous other disruptions in the axial magma lens reflection and undulations in magma lens depth over short spatial scales that define magma lens segments ~ 5–20 km in length (Carbotte et al., 2011). Discontinuities in the seafloor structures defining the axial zone (the AST and axial pillow ridges) are present above many of the magma lens disruptions. Pinches and swells of the axial high are observed to be coincident with magma lens segmentation, suggesting a persistent segmentation for thousands to tens of thousands of years.

Beneath the 17 km long region of the EPR where new lavas erupted in 2005 and 2006 (Soule et al., 2007), three lens segments are identified, defined by magma lens discontinuities at 9°44'–9°45'N, 9°48'–9°48.5'N, and 9°50.5'N, with the latter being a less well-defined zone of offset. Comparison of 2D images from data obtained in 1985 (Kent et al., 1993a) with coincident 3D data from 2008 suggests that the eruption preferentially drained more distal regions of the central lens segment (Mutter et al., 2009). The width of the magma lens in the eruption area (500–700 m) is narrower than anywhere else along this stretch of the EPR, except near small nontransform discontinuities (Kent et al., 1993a,b, 2000), and perhaps surprisingly, there is no evidence that a wide lens is linked to areas of enhanced magmatic activity. Indeed, the widest magma lens (4.5 km) imaged to date globally is found just to the north of the 9°03'N overlapping spreading center (OSC) discontinuity (Kent et al., 2000). The presence of a wide magma body in this region has been attributed to lateral
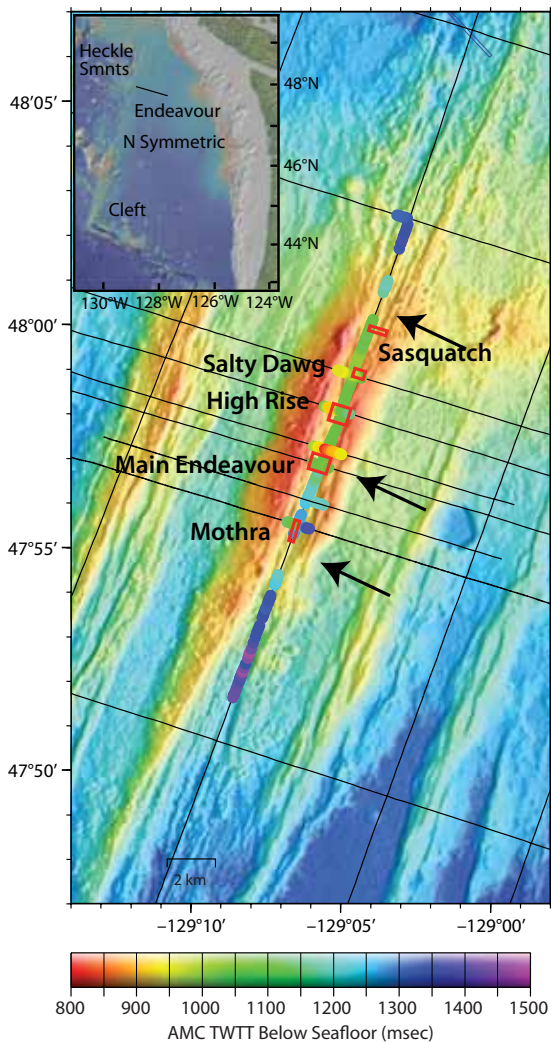

Figure 2. Map of Endeavour Segment showing the depth to the magma lens reflection beneath the seafloor in two-way travel time (TWTT) measured from along-axis and cross-axis seismic profiles. Red boxes indicate the locations of major vent fields. Black arrows indicate the interpreted segment boundaries. The inset shows the location of Endeavour and other ridge segments of the Juan de Fuca Ridge referenced in the text. The black line in the inset indicates the location of the FlankFlux transect, where basement temperatures were measured in nine Ocean Drilling Program boreholes to estimate heat flow in order to constrain fluid transport. AMC = axial magma chamber.

offset of the lower crustal melt supply relative to the zone of dike intrusion (Kent et al., 1993b; Combier et al., 2008). Magma may reside in this mid-crust magma body for longer periods between eruptions, compared with the actively erupting region at 9°46'–9°51'N, where a narrow lens is found.

Studies of the melt content of the magma lens in the EPR area are limited to two investigations of the 1985 data at 9°39'N, from which a fully (Collier and Singh, 1997) to partially (Hussenoeder et al., 1996) molten lens is inferred. New studies using the 2008 data indicate variations in magma crystallinity along the axis (Xu et al., 2010). The new data also reveal reflection events in the mid-crust beneath the AMC (Figure 1b), and studies of the potential origin of these events (internal multiples, converted phases, or distinct mid to lower crustal lenses) are underway.

The main clusters of hydrothermal venting within the EPR ISS (at 9°49'–9°50'N and ~ 9°45'–9°47'N; Figure 1B; e.g., Fornari et al., 2004) are underlain by two magma lens segments, indicating distinct heat sources that may contribute to the differences in the temporal evolution and fluid chemistry of these vents (Von Damm, 2004). As at Endeavour Segment, all other known high-temperature vents in the region are underlain by a magma lens reflection.

Notably, as at Endeavour Segment, enhanced ridge-axis melt production linked to the presence of a nearby mantle melt anomaly may contribute to localization of magmatism at the EPR site. The Lamont Seamounts are located immediately west of the EPR "bull's-eye" (9°49'–9°51'N; Fornari et al., 1984). Within the bull's-eye region,

the ridge axis and the underlying mid-crust magma lens are locally shallow, indicating an elevated axial thermal regime; hydrothermal venting is clustered; and erupted lavas have the highest Mg number along the ridge axis (Perfit et al., 1994; Goss et al., 2010). The two documented volcanic eruptions of 1991–92 (Haymon et al., 1993; Rubin et al., 1994) and 2005–06 (Tolstoy et al., 2006; Cowen et al., 2007; Soule et al., 2007) were both sourced from approximately the same site, and the locations of hydrothermal venting persisted through these eruptions. An important prediction of the influence of ridge-melt anomaly interaction at these sites is that these regions of locally enhanced axial magmatism and hydrothermal venting are likely to persist for long time periods (tens to hundreds of thousands of years).

Structure of Seismic Layer 2A and Inferences for Construction of the Upper Crust and Hydrothermal Alteration Within the Axial Zone

With the 6 km long hydrophone streamers employed for both the EPR and Endeavour surveys, excellent information on the geometry and velocity structure of the uppermost layer of the oceanic crust—seismic Layer 2A—has been obtained for each region. Studies of the structure of Layer 2A provide insights into the volcanic construction and post-accretion modification of the upper crust (e.g., Harding et al., 1993; Grevemeyer and Bartetzko, 2004; Christeson et al., 2007).

At Endeavour Segment, the thickness of seismic Layer 2A varies considerably along the axis, from 180 to 630 m (150 to 400 ms; Van Ark et al., 2007), with an average of 380 m ± 120 m. As

at other ridges, Layer 2A is thinnest in the central part of the segment where the AMC is detected, and it thickens to the north and south where the AMC is absent. In contrast to observations at the fast-spreading EPR (e.g., Harding et al., 1993) and the more magmatically robust Cleft segment of the JdFR south of Endeavour (Canales et al., 2005), no clear pattern of off-axis thickening is observed. The mean thickness of Layer 2A on the ridge flanks determined from the ridge axis survey is 500 ± 110 m (380 ± 90 ms). Velocity modeling of common mid-point gathers indicates uppermost Layer 2A increase by 10–20% within a few kilometers off axis (Van Ark et al., 2007; Nedimović et al., 2008), which is attributed to crack closure and infill of volcanic porosity by precipitation of alteration minerals during hydrothermal circulation.

Along the EPR axis, seismic Layer 2A is thinner than at Endeavour Segment (155 m ± 53 m), thickening toward the 9°03'N OSC and the bounding transform faults. Local thickening is also observed at the 8°37'N OSC and north of 9°50'N. In contrast to Endeavour Segment, Layer 2A at the EPR thickens markedly away from the axis, approximately doubling in thickness in 1–3 km (Harding et al., 1993; Christeson et al., 1996). This off-axis doubling is attributed to accumulation of the extrusive layer via thin, possibly high-effusion-rate, flows that can travel up to several kilometers from their eruptive fissures at the axis (Harding et al., 1993; Hooft et al., 1996). The lack of off-axis thickening of Layer 2A at Endeavour Segment implies less off-axis transport of lava flows, perhaps due to damming of flows by the bounding axial

graben walls. As at Endeavour Segment, lower P-wave velocities are observed on axis at the EPR; they increase off axis, presumably due to crack closure and hydrothermal precipitation.

Discovery of Multiple Near- and Off-Axis Magma Bodies In and Below the Crust

A commonly accepted view of mid-ocean ridge magmatism during the last two decades has been that melt arising from the mantle beneath intermediate to ultrafast mid-ocean ridges is focused within a narrow region at the ridge axis. At crustal levels, this axial accretionary zone is composed of a thin ~ 1 km wide magma lens of partial to pure melt and a 4–6 km wide zone of low velocities in the lower crust attributed to crystal mush and hot rock (e.g., Vera et al., 1990; Kent et al., 1993a; Dunn et al., 2000). However, a growing number of studies surveying near- and off-axis regions have found geophysical, geological, and geochemical indications of magmatism well beyond the ridge axis. Those lines of evidence include: (1) P-S conversions indicating melt sills at the base of the crust 22 km west of the EPR (Garmany, 1989), and (2) detection of seismic-wave diffraction and P- to S-wave (P-S) conversions, indicating a magma body in the mid-crust overlying an anomalously hot lower crust 20 km east of the EPR axis (Durant and Toomey, 2009). In addition, there is radiogenic isotope evidence of "zero-age" volcanic eruptions at distances up to 4 km from the EPR (Goldstein et al., 1994; Sims et al., 2003), and there are anomalously young eruptions as much as 30 km from the EPR axis (Zou et al., 2002; Turner et al., 2011).

The 2008 3D MCS experiment at the EPR ISS has produced the best-located and most unambiguous evidence to date of magma currently accumulating off axis in molten lenses within the crust at fast-spreading mid-ocean ridges. This experiment imaged a network of off-axis melt bodies located outside of, but connected to, the axial low-velocity zone, 4–8 km east of the ridge axis at 9°52'–9°55'N and at depths up to 4.2 km below the seafloor (Canales, in press; see Figure 1 in Canales et al., 2012, in this issue). These bodies and others imaged in the survey area, when viewed in the context of morphological and petrological information for this section of the EPR, suggest that some off-axis magmatic systems develop in associa-tion with axial discontinuities, and that in cases when they are close enough to the ridge axis (< 10 km), they may influence the eruptive style of the axial system by reducing the availability of melt for the axial region. The volume of crustal production associated with off-axis magmatism is expected to be modest as there is no evidence for a significant increase in crustal thickness away from the ridge axis (e.g., Barth and Mutter, 1996). However, off-axis magmatism may play an important role in seafloor characteristics. The imaged off-axis crustal magmatic bodies could be the source of enriched basalts as well as the more-evolved lavas, which are more prevalent in off-axis than in axial samples (Perfit et al., 1994, and 2012, in this issue; Waters et al., 2011). Evidence for off-axis hydrothermal venting in the form of mineral deposits and vent fauna has been discovered along young abyssal hills at ~ 10°20'N and 9°20'N (Haymon et al., 2005; R. Haymon, University of

California, Santa Barbara, *pers. comm.,* 2011). The imaged off-axis melt bodies provide candidate heat sources for driving focused off-axis hydrothermal venting, although investigations of the imaged sites for venting have not yet been conducted.

Local magma accumulations beneath the crust at mid-ocean ridges have long been inferred from observations of ophiolites and from geophysical studies primarily within the EPR 9°–10°N region. Seismic tomography, supported by seafloor compliance studies, provide evidence for a 15–20 km wide region of partial melt beneath the crust (Crawford et al., 1999; Dunn et al., 2000). Mapping in ophiolites show a crust-mantle boundary or Moho Transition Zone (MTZ) composed of gabbro sills intruded into mantle rocks that vary in thickness from a few meters to several kilometers in scale (e.g., Boudier and Nicolas, 1995). While the Mohorovičić (Moho) discontinuity is typically imaged in reflection studies as a single event of variable strength (e.g., Kent et al., 1994; Barth and Mutter, 1996), data from the flanks of the JdFR provide the first seismic reflection images of localized magma sills within the MTZ, consistent with a thick MTZ (Figure 3; Nedimović et al., 2005). Clusters of bright reflection events are imaged, which are attributed to both frozen and partially molten gabbro lenses embedded within mantle rocks. Those imaged further from the ridge axis (> 5–10 km away) have been inferred to be frozen, while those closer to the ridge axis may represent partial melts. The most prominent clusters of MTZ reflections, imaged ~ 33 km away from the ridge axis, are up to 4–5 km long with a combined thickness of over

2,000 m and are found adjacent to the wakes left by propagating ridges on the flanks of the JdFR. These sills are inferred to have formed on axis, at the tip of the propagating ridge segment, by intrusion of melt at the base of the crust as spreading breaks into pre-existing lithosphere. They are the presumed remnants of magma source bodies for the more differentiated Fe-rich rocks typically found at propagating ridges (Sinton et al., 1983)

While the new observations described above indicate that multiple magma reservoirs contribute to building crust over a wider and deeper zone than previously appreciated, evidence for magma sills at different levels in the crust right at the axis has not yet been found. A 3D MCS study of the EPR 9°03'N OSC (Singh et al., 2006) observed Moho reflections and evidence for high melt content within the lower crust directly beneath the axial shallow melt sill, but no discrete lower crustal sills were observed. The lack of seismic evidence for lower crustal sills at the axis does not rule out the possibility of sills smaller than can be resolved with the 10–15 Hz dominant frequency seismic sources used (< ~ 50 m thick by < 250 m wide). In addition, lower crustal sills could be present but obscured by a combination of the negative effects on reflection imaging of large lateral velocity variations and high attenuation caused by the presence of the mid-crustal magma lens and interstitial melt within the lower crust. Application of advanced imaging techniques (such as wave-equation datuming and pre-stack depth migration) has the potential to resolve this ambiguity.

It is also possible that lower crustal

sills do not develop right at the ridge axis but instead form at or near the edges of the axial low-velocity zone. Evidence for this interpretation comes from MCS data collected at the Cleft segment of the southern JdFR (see Figure 2 inset). Here, 2D MCS data imaged a prominent reflection at 5–6 km depth extending ~ 2.4 km and ~ 1.8 km in the ridge-parallel and ridge-perpendicular directions, respectively, interpreted as a lower crustal melt lens (Figure 4; Canales et al., 2009). This reflector is located 1.4–3.2 km east

of the axis, near the edge of the axial accretionary zone (assuming a width of 4–6 km from the EPR studies; Dunn et al., 2000). This deep sill also coincides with a positive anomaly in crustal travel times to Moho, indicating local crustal thickening and/or presence of melt within the lower crust. The presence of this deep melt lens implies that permeability boundaries can develop in the lower crust, at least near the boundaries of the axial low-velocity zone, providing support for ophiolite-based models
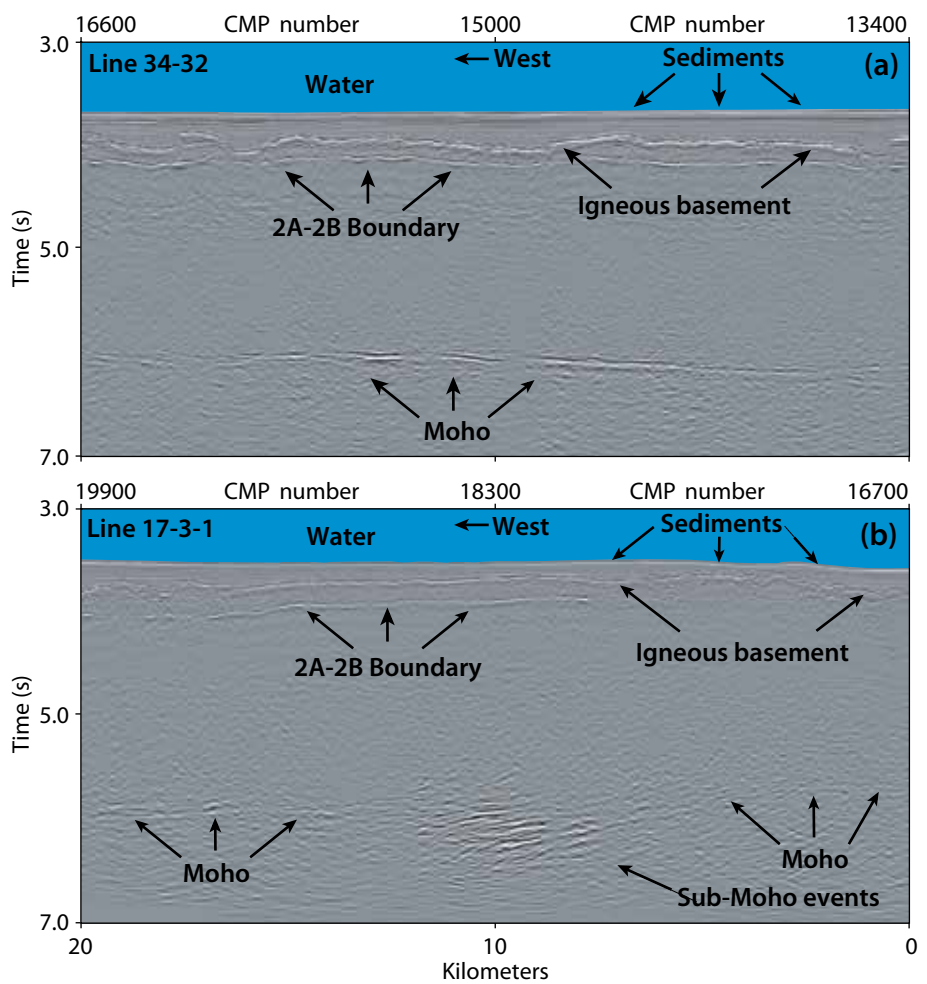

Figure 3. Seismic reflection structure of oceanic crust from two ridge flank regions showing (a) a bright Moho reflection, and (b) a local zone with clusters of bright reflections interpreted as sills within the Moho Transition Zone. Panel (a) is from the east flank of Northern Symmetric Segment, Juan de Fuca Ridge. Panel (b) is from the east flank of Endeavour Segment. *From Nedimović et al. (2005)*

that propose the lower oceanic crust is built from multiple magma bodies emplaced at multiple levels in the crust (Kelemen et al., 1997).

Crustal Evolution After Formation and Ridge Flank Hydrothermal Flow

The post-emplacement evolution of oceanic crust has important implications for understanding energy and mass exchange between the ocean and Earth's interior, and for studying the relationship between oceanic plate hydration and subduction zone processes. Although there has been considerable work in the past few decades dedicated to characterizing the evolution of the upper crust, most studies have been based on sparse observations of seismic Layer 2A with little analysis of Layer 2B (e.g., Cudrak and Clowes, 1993; Harding et al., 1993; Rohr, 1994;

Grevemeyer et al., 1999; Grevemeyer and Bartetzko, 2004; Christeson, 2007). Using the 2002 JdFR MCS data, the most detailed investigation of Layer 2A evolution to date was conducted as well as the first study focused on processes that affect uppermost Layer 2B after formation (Nedimović et al., 2008; Newman et al., 2011).

Results show that Layers 2A and 2B evolve in different ways. As observed elsewhere, a small increase in Layer 2A velocity occurs rapidly near the ridge axis, presumably linked to high-temperature axial hydrothermal flow, followed by a more gradual evolution for many millions of years due to passive, low-temperature hydrothermal circulation (see Grevemeyer and Bartetzko, 2004, and references therein). On the flanks of the JdFR, Layer 2A velocities increase from < 2.5 km s^{-1} at the ridge axis to > 4.0 km s^{-1} in mature crust

5–8 million years old (Nedimović et al., 2008). Following a different course from Layer 2A, seismic Layer 2B evolves rapidly within the first 0.5 million years after crustal formation, with upper Layer 2B velocities increasing on average by 0.8 km s^{-1}, reaching an approximately constant velocity of 5.2 ± 0.3 km s^{-1} in older crust (Newman et al., 2011). Unlike for Layer 2A, the strongest impact on Layer 2B evolution may be mineral precipitation due to active hydrothermal circulation centered about the ridge crest and driven by heat from the axial magma chamber and associated intrusive bodies.

Comparison between Layer 2B velocities and hydrothermal circulation patterns, inferred from heat flow, fluid flow, and pore fluid geochemistry data, reveals correlation of both upflow or discharge zones with 2B velocity lows and downflow or recharge zones with 2B velocity highs (Figure 5; Newman et al., 2011). This relationship is attributed to enhanced pore clogging within upper Layer 2B within the downflow zones. In the vicinity of the ridge axis, where there is no or little sedimentary cover, upflow zones are collocated with seafloor topographic highs and downflow zones with topographic lows. Further away from the ridge axis, in areas where sediments fill in lows to form minibasins, some of the seafloor highs appear to have been converted to downflow zones, indicating that both seafloor relief and sedimentary cover affect hydrothermal flow and therefore mineral precipitation (Figure 5). Sediment cover is also found to have a major impact on Layer 2A evolution. For the flanks blanketed with a continuous, sealing sedimentary cover, Layer 2A increases velocity at about twice the rate observed for ridge flanks
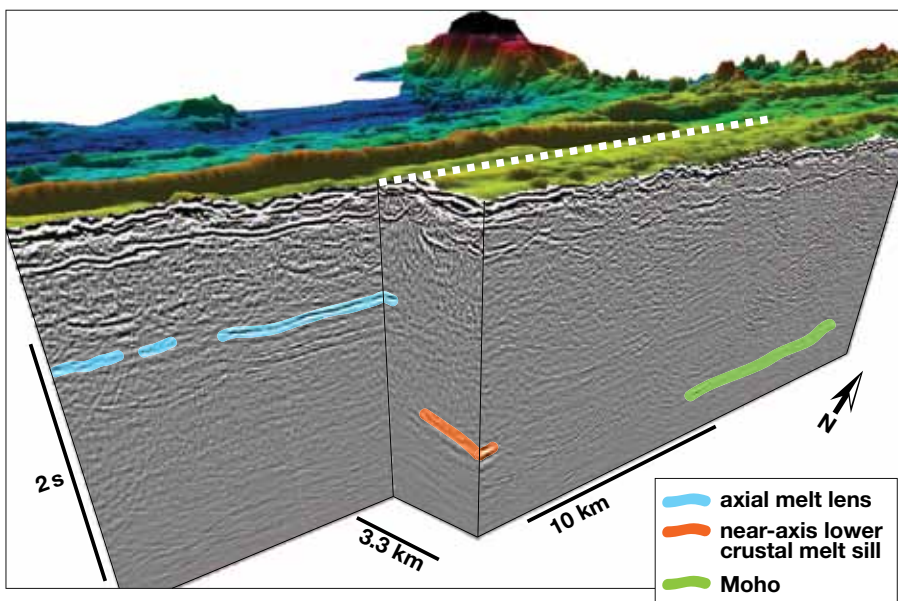

Figure 4. Three-dimensional perspective of crustal structure along the axis and near axis flanks of the Juan de Fuca Ridge Cleft Segment showing an isolated melt lens in the lower crust (orange) located ~ 1–3 km away from the axial melt lens (blue). Moho (green) is not imaged directly beneath the lower crustal melt sill or the ridge axis. The white dashed line indicates the spreading axis. *From Canales et al. (2009)*

with sparse or discontinuous sediment cover (Nedimović et al., 2008). The correlation between Layer 2A velocity and sediment cover is attributed to more rapid precipitation of alteration minerals in the porous upper crust as the hydrothermal regime evolves from one dominated by open exchange with the water column to a regime that is effectively closed to seawater exchange by the sealing sedimentary blanket.

SUMMARY AND FUTURE DIRECTIONS

Studies of crustal structure at the Endeavour and EPR Integrated Study Sites conducted under the Ridge 2000 Program reveal important new insights into crustal accretion and hydrothermal flow at mid-ocean ridges while also providing an integrating framework for the diverse multidisciplinary investigations underway at these sites. In this final section, we summarize the primary findings with a focus on new questions arising and potential directions for future investigation.

1. With the discovery of a mid-crust magma body beneath much of the axial zone and underlying all known vent fields at both the JdFR and the EPR ISSs, a similar framework for volcanic construction of the crust and hydrothermal flow has emerged for both of these intermediate and fast spreading ridges. However, important questions remain concerning the feedbacks and linkages between tectonic and magmatic processes, and the influence of faulting on the geometry of hydrothermal flow at the more extensively tectonized Endeavour Segment.

2. Evidence for small-scale (5–20 km) segmentation of the axial magma lens is found at both the EPR and Endeavour sites, with implications for magma evolution and the chemistry of erupted lavas, and for the geometry of hydrothermal circulation in the upper crust. While this segmentation can be confidently interpreted in the 3D MCS data set now available for the EPR site, the presence of segmentation remains speculative at Endeavour due to the

inherent limitations of the existing sparse 2D data set. Future 3D seismic imaging will be needed there to establish the detailed geometry and nature of the segmentation as well as its relationship to seafloor tectonic, volcanic, and hydrothermal features.

3. Three-dimensional images of magma systems at the EPR now achieve a spatial resolution that permits direct comparison of features at the seafloor, such as
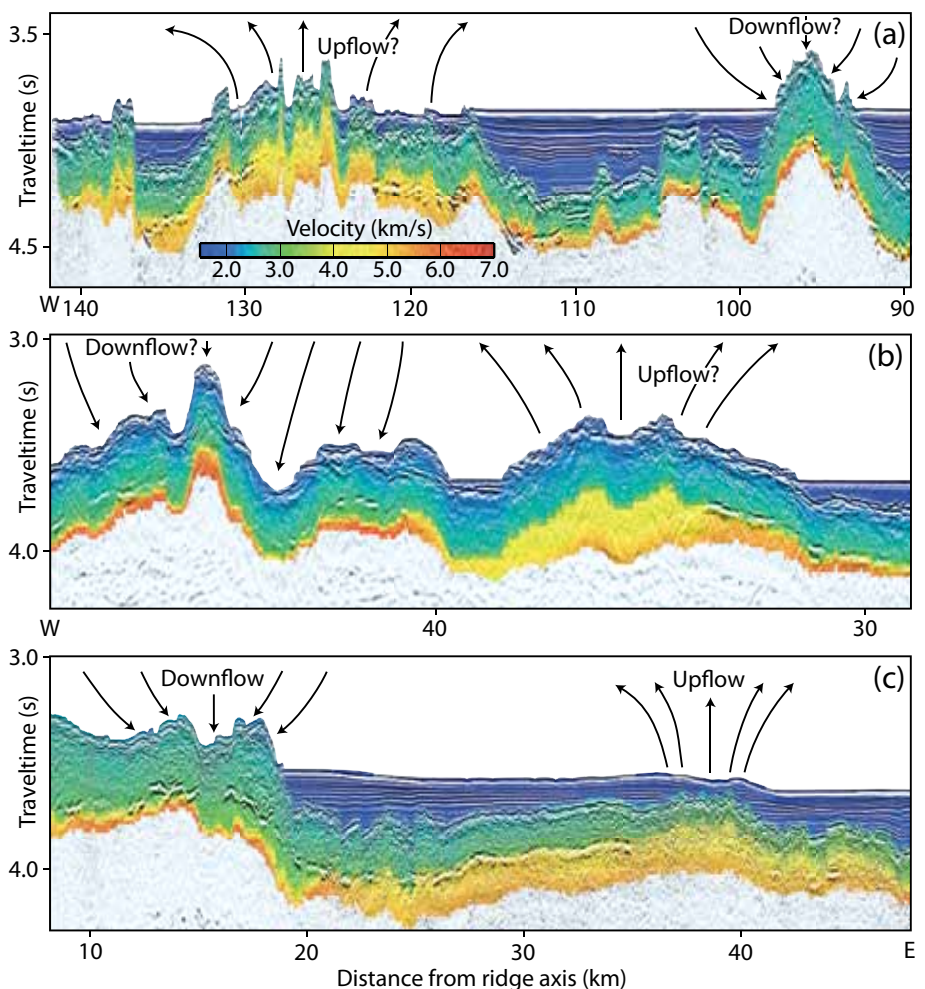

Figure 5. Composite seismic reflection and P-wave tomographic images of three pairs of basement highs separated by sedimentary minibasins that may be guiding hydrothermal discharge and recharge on the flanks of the Juan de Fuca Ridge. The three examples shown are from (a) western Endeavour flank, (b) western Northern Symmetric flank, and (c) eastern Endeavour flank. Arrows mark the inferred (panels a and b) or measured (panel c, from the Ocean Drilling Program FlankFlux transect) upflow and downflow zones. *From Newman et al. (2011)*

hydrothermal venting that responds to the magma's thermal forcing. The next challenge is to understand the temporal evolution of magma systems, including changes in segmentation geometry, foci of eruption, and inflation/deflation periods. On-bottom geodetic studies, repeat seafloor compliance measurements, and time-lapse, repeat 3D (see Canales et al., 2012, in this issue) seismic imaging may allow temporal changes to be mapped and provide an understanding of magma dynamics.

4. As local heat sources on the ridge flanks, off-axis magma bodies may underlie sites of off-axis hydrothermal venting, such as those discovered by Haymon et al. (2005). However, with existing data essentially providing a snapshot in time, the longevity of off-axis melt lenses and the temporal variations in their spatial distribution are unknown. Moreover, whether they are sources of high-temperature circulation on the ridge flanks is only conjecture at present. Seafloor observations above these features are needed to establish the presence and determine the nature of hydrothermal circulation and off-axis seafloor volcanism potentially associated with these magmatic systems.

5. Detailed new information on the velocity structure of the upper crust indicates a different evolutionary course for Layers 2A and 2B as they age. Correlation between the variations in upper crustal velocities and known hydrothermal circulation patterns inferred from heat flow, direct fluid flow, and pore fluid geochemistry data reveals the potential of long-streamer MCS techniques to remotely determine

the patterns of hydrothermal flow within the upper oceanic crust. Additional work is needed to confirm this finding. Longer streamers (> 6 km) and dense ocean-bottom seismometer arrays (< 3 km spacing) would extend our understanding of crustal evolution to layers found at depths greater than that of upper Layer 2B.

ACKNOWLEDGEMENTS

REFERENCES

Barth, G.A., and J.C. Mutter. 1996. Variability in oceanic crustal thickness and structure: Multichannel seismic reflection results from the northern East Pacific Rise. *Journal of Geophysical Research* 101:17,951–17,975, http://dx.doi.org/10.1029/96JB00814.

Boudier, F., and A. Nicolas. 1995. Nature of the Moho transition zone in the Oman ophiolite. *Journal of Petrology 36*:777–796, http://petrology.oxfordjournals.org/content/36/3/777.abstract (accessed December 21, 2011).

Carbotte, S.M., R.S. Detrick, J.P. Canales, A.J. Harding, G.M. Kent, J. Babcock, M.R. Nedimović, J.B. Diebold, and E. van Ark. 2006. Magmatic-tectonic episodicity at oceanic spreading centers revisited. *Geology* 34:209–212, http://dx.doi.org/10.1130/G21969.1.

Carbotte, S.M., M. Marjanovic, H.D. Carton, J.C. Mutter, J.P. Canales, M. Xu, M.R. Nedimović, and O. Aghaei. 2011. The ups and downs of magma in the crust beneath the East Pacific Rise axis 8°20′–10°10′N. *Eos, Transactions, American Geophysical Union* Fall Meeting Abstract OS22A-01.

Carbotte, S.M., M.R. Nedimović, J.P. Canales, G.M. Kent, A.J. Harding, and M. Marjanovic. 2008. Variable crustal structure along the Juan de Fuca Ridge: Influence of on-axis hotspots and absolute plate motions. *Geochemistry Geophysics Geosystems 9,* Q08001, http://dx.doi.org/10.1029/2007GC001922.

Canales, J.P., H. Carton, S.M. Carbotte, J.C. Mutter, M.R. Nedimović, M. Xu, O. Aghaei, M. Marjanović, and K. Newman. In press. Network of off-axis melt bodies at the East Pacific Rise. *Nature Geoscience.*

Canales, J.P., H. Carton, J.C. Mutter, A. Harding, S.M. Carbotte, and M.R. Nedimović. 2012. Recent advances in multichannel seismic imaging for academic research in deep oceanic environments. *Oceanography* 25(1):113–115, http://dx.doi.org/10.5670/oceanog.2012.09.

Canales, J.P., R.S. Detrick, S.M. Carbotte, G.M. Kent, J.B. Diebold, A.J. Harding, J. Babcock, M.R. Nedimović, and E. van Ark. 2005. Upper crustal structure and axial topography at intermediate-spreading ridges: Seismic constraints from the southern Juan de Fuca Ridge. *Journal of Geophysical Research* 110, B12104, http://dx.doi.org/12110.11029/12005JB003630.

Canales, J.P., M.R. Nedimović, G.M. Kent, S.M. Carbotte, and R.S. Detrick. 2009. Seismic reflection images of a near-axis melt sill within the lower crust at the Juan de Fuca Ridge. *Nature* 460:89–93, http://dx.doi.org/10.1038/nature08095.

Canales, J.P., S.C. Singh, R.S. Detrick, S.M. Carbotte, A.J. Harding, G.M. Kent, J.B. Diebold, J. Babcock, and M.R. Nedimović. 2006. Seismic evidence for variations in axial magma chamber properties along the southern Juan de Fuca Ridge. *Earth and Planetary Science Letters* 246:353–366, http://dx.doi.org/10.1016/j.epsl.2006.04.032.

Carton, H.D., S.M. Carbotte, J.C. Mutter, J. Canales, M.R. Nedimović, O. Aghaei, M. Marjanović, and K.R. Newman. 2010. Three-dimensional seismic reflection images of axial melt lens and seismic Layer 2A between 9°42′N and 9°57′N on the East Pacific Rise. *Eos, Transactions, American Geophysical Union* 90:Fall Meeting Abstract OS21C-1514.

Christeson, G.L., G.M. Kent, G.M. Purdy, and R.S. Detrick. 1996. Extrusive thickness variability at the East Pacific Rise, 9°–10°N: Constraints from seismic techniques. *Journal of Geophysical Research* 101:2,859–2,873, http://dx.doi.org/10.1029/95JB03212.

Christeson, G.L., K.D. McIntosh, and J.A. Karson. 2007. Inconsistent correlation of seismic Layer 2a and lava layer thickness in oceanic crust. *Nature* 445:418–421, http://dx.doi.org/10.1038/nature05517.

Collier, J.S., and S.C. Singh. 1997. Detailed structure of the top of the melt body beneath the East Pacific Rise at 9°40′N from waveform inversion of seismic reflection data. *Journal of Geophysical Research* 102:20,287–20,304, http://dx.doi.org/10.1029/97JB01514.

Combier, V., S.C. Singh, M. Cannat, and J. Escartin. 2008. Mechanical decoupling and thermal structure at the East Pacific Rise axis 9°N:

Constraints from axial magma chamber geometry and seafloor structures. *Earth and Planetary Science Letters* 272:19–28, http://dx.doi.org/10.1016/j.epsl.2008.03.046.

Cowen, J.P., B. Glazer, D.J. Fornari, T.M. Shank, S.A. Soule, B. Love, A. Treusch, K.R. Pomanig, R.C. Holmes, M. Tolstoy, and E.T. Baker. 2007. Volcanic eruptions at East Pacific Rise near 9°50'N. *Eos, Transactions, American Geophysical Union* 88(7):81, http://dx.doi.org/10.1029/2007EO070001.

Crawford, W.C., and S.C. Webb. 2002. Variations in the distribution of magma in the lower crust and at the Moho beneath the East Pacific Rise at 9°–10°N. *Earth and Planetary Science Letters* 203:117–130, http://dx.doi.org/10.1016/S0012-821X(02)00831-2.

Crawford, W.C., S.C. Webb, and J.A. Hilderbrand. 1999. Constraints on melt in the lower crust and Moho at the East Pacific Rise using seafloor compliance measurements. *Journal of Geophysical Research* 104:2,923–2,939, http://dx.doi.org/10.1029/1998JB900087.

Cudrak, C.F., and R.M. Clowes. 1993. Crustal structure of Endeavour Ridge Segment, Juan de Fuca Ridge, from a detailed seismic refraction survey. *Journal of Geophysical Research* 98:6,329–6,349, http://dx.doi.org/10.1029/92JB02860.

Detrick, R.S., P. Buhl, E.E. Vera, J.C. Mutter, J.A. Orcutt, J.A. Madsen, and T.M. Brocher. 1987. Multi-channel seismic imaging of a crustal magma chamber along the East Pacific Rise. *Nature* 326:35–41, http://dx.doi.org/10.1038/326035a0.

Dunn, R.A., and D.R. Toomey. 1997. Seismological evidence for three-dimensional melt migration beneath the East Pacific Rise. *Nature* 388:259–262, http://dx.doi.org/10.1038/40831.

Dunn, R.A., D.R. Toomey, and S.C. Solomon. 2000. Three-dimensional seismic structure and physical properties of the crust and shallow mantle beneath the East Pacific Rise at 9°30'N. *Journal of Geophysical Research* 105:23,537–23,555, http://dx.doi.org/10.1029/2000JB900210.

Durant, D.T., and D.R. Toomey. 2009. Evidence and implications of crustal magmatism on the flanks of the East Pacific Rise. *Earth and Planetary Science Letters* 287:130–136, http://dx.doi.org/10.1016/j.epsl.2009.08.003.

Fornari, D.J., K.L. Von Damm, J.G. Bryce, J.P. Cowen, V. Ferrini, A. Fundis, M.D. Lilley, G.W. Luther III, L.S. Mullineaux, M.R. Perfit, and others. 2012. The East Pacific Rise between 9°N and 10°N: Twenty-five years of integrated, multidisciplinary oceanic spreading center studies. *Oceanography* 25(1):18–43, http://dx.doi.org/10.5670/oceanog.2012.02.

Fornari, D.J., R.M. Haymon, M.R. Perfit, T.K.P. Gregg, and M.H. Edwards. 1998. Axial summit trough of the East Pacific Rise 9°–10°N: Geological characteristics and evolution of the axial zone on fast spreading mid-ocean ridges. *Journal of Geophysical Research* 103:9,827–9,855, http://dx.doi.org/10.1029/98JB00028.

Fornari, D.J., W.B.F. Ryan, and P.J. Fox. 1984. The evolution of craters and calderas on young seamounts: Insights from Sea MARC I and Sea Beam sonar surveys of a small seamount group near the axis of the East Pacific Rise at 10°N. *Journal of Geophysical Research* 89:11,069–11,083.

Garmany, J. 1989. Accumulations of melt at the base of young oceanic crust. *Nature* 340:628–632, http://dx.doi.org/10.1038/340628a0.

Glickson, D.A., D.S. Kelley, and J.R. Delaney. 2007. Geology and hydrothermal evolution of the Mothra Hydrothermal Field, Endeavour Segment, Juan de Fuca Ridge. *Geochemistry Geophysics Geosystems* 8, Q06010, http://dx.doi.org/10.1029/2007GC001588

Goldstein, S.J., M.R. Perfit, R. Batiza, D.J. Fornari, and M.T. Murrell. 1994. Off-axis volcanism at the East Pacific Rise detected by uranium-series dating of basalts. *Nature* 367:157–159, http://dx.doi.org/10.1038/367157a0.

Goss, A.R., M.R. Perfit, W.I. Ridley, K.H. Rubin, G.D. Kamenov, S.A. Soule, A. Fundis, and D.J. Fornari. 2010. Geochemistry of lavas from the 2005–2006 eruption at the East Pacific Rise, 9°46'N–9°56'N: Implications for ridge crest plumbing and decadal changes in magma chamber compositions. *Geochemistry Geophysics Geosystems* 11, Q05T09, http://dx.doi.org/10.1029/2009GC002977.

Grevemeyer, I., and A. Bartetzko. 2004. Hydrothermal activity and ageing of oceanic crust. Pp. 128–150 in *Hydrogeology of the Oceanic Lithosphere*. E.E. Davis and H. Elderfield, eds, Cambridge University Press.

Grevemeyer, I., N. Kaul, H. Villinger, and W. Weigel. 1999. Hydrothermal activity and the evolution of the seismic properties of upper oceanic crust. *Journal of Geophysical Research* 104:5,069–5,079, http://dx.doi.org/10.1029/1998JB900096.

Harding, A.J., G.M. Kent, and J.A. Orcutt. 1993. A multichannel seismic investigation of upper crustal structure at 9°N on the East Pacific Rise: Implications for crustal accretion. *Journal of Geophysical Research* 98:13,925–13,944, http://dx.doi.org/10.1029/93JB00886.

Haymon, R.M., D.J. Fornari, M. Edwards, S.M. Carbotte, D. Wright, and K.C. Macdonald. 1991. Hydrothermal vent distribution along the East Pacific Rise crest (9°09'–9°54'N) and its relationship to magmatic and tectonic processes on fast spreading mid-ocean ridges. *Earth and Planetary Science Letters* 104:513–534, http://dx.doi.org/10.1016/0012-821X(91)90226-8.

Haymon, R.M., D.J. Fornari, K.L. Von Damm, M.D. Lilley, M.R. Perfit, J.M. Edmond, W.C. Shanks III, R.A. Lutz, J.M. Grebmeier, S. Carbotte, and others. 1993. Volcanic eruption of the mid-ocean ridge along the East Pacific Rise crest at 9°45–52'N: Direct submersible observations of seafloor phenomena associated with an eruption event in April, 1991. *Earth and Planetary Science Letters* 119:85–101, http://dx.doi.org/10.1016/0012-821X(93)90008-W.

Haymon, R.M., K.C. Macdonald, S.B. Benjamin, and C.J. Ehrhardt. 2005. Manifestations of hydrothermal discharge from young abyssal hills on the fast-spreading East Pacific Rise flank. *Geology* 33:153–156, http://dx.doi.org/10.1130/G21058.1.

Hussenoeder, S.A., J.A. Collins, G.M. Kent, R.S. Detrick, and the TERA Group. 1996. Seismic analysis of the axial magma chamber reflector along the southern East Pacific Rise from conventional reflection profiling. *Journal of Geophysical Research* 101:22,087–22,105, http://dx.doi.org/10.1029/96JB01907.

Kappel, E.S., and W.B.F. Ryan. 1986. Volcanic episodicity and a non-steady state rift valley along the Northeast Pacific spreading centers: Evidence from Sea MARC I. *Journal of Geophysical Research* 91:13,925–13,940, http://dx.doi.org/10.1029/JB091iB14p13925.

Kelemen, P.B., K. Koga, and N. Shimizu. 1997. Geochemistry of gabbro sills in the crust-mantle transition zone of the Oman ophiolite: Implications for the origin of the oceanic lower crust. *Earth and Planetary Science Letters* 146:475–488, http://dx.doi.org/10.1016/S0012-821X(96)00235-X.

Kelley, D.S., S.M. Carbotte, D.W. Caress, D.A. Clague, J.R. Delaney, J.B. Gill, H. Hadaway, J.F. Holden, E.E.E. Hooft, J.P. Kellogg, and others. 2012. Endeavour Segment of the Juan de Fuca Ridge: One of the most remarkable places on Earth. *Oceanography* 25(1):44–61, http://dx.doi.org/10.5670/oceanog.2012.03.

Kent, G.M., A.J. Harding, and J.A. Orcutt. 1993a. Distribution of magma beneath the East Pacific Rise between the Clipperton Transform and the 9°17'N Deval from forward modeling of common depth point data. *Journal of Geophysical Research* 98:13,945–13,969, http://dx.doi.org/10.1029/93JB00705.

Kent, G.M., A.J. Harding, and J.A. Orcutt. 1993b. Distribution of magma beneath the East Pacific Rise near the 9°03'N overlapping spreading center from forward modeling of common depth point data. *Journal of Geophysical Research* 98:13,971–13,995, http://dx.doi.org/10.1029/93JB00706.

Kent, G.M., A.J. Harding, J.A. Orcutt, R.S. Detrick, J.C. Mutter, and P. Buhl. 1994. The uniform accretion of oceanic crust south of the Garrett Transform at 14°15'S on the East Pacific Rise. *Journal of Geophysical Research* 99:9,097–9,116.

Kent, G.M., S.C. Singh, A.J. Harding, M.C. Sihna, J.A. Orcutt, P.J. Barton, R.S. White, S. Bazin, R.W. Hobbs, C.H. Tong, and J.W. Pye. 2000. Evidence from three-dimensional seismic reflectivity images for enhanced melt supply beneath mid-ocean ridge discontinuities. *Nature* 406:614–618, http://dx.doi.org/10.1038/35020543.

Key, K., S. Constable, J. Behrens, G. Heinson, and C. Weiss. 2005. Mapping the northern EPR magmatic system using marine EM. *Ridge 2000 Events* 3:35–37.

Mottl, M.J. 2003. Partitioning of energy and mass fluxes between mid-ocean ridge axes and flanks at high and low temperature. Pp. 271–286 in *Energy and Mass Transfer in Marine Hydrothermal Systems*. P. Halbach, V. Tunnicliffe, and J.R. Hein, eds, Dahlem University Press.

Mutter, J.C., S.M. Carbotte, M. Nedimović, J.P. Canales, and H. Carton. 2009. Seismic imaging in three dimensions on the East Pacific Rise. *Eos, Transactions, American Geophysical Union* 90(42):374–375, http://dx.doi.org/10.1029/2009EO420002.

Nedimović, M., S.M. Carbotte, J.B. Diebold, A.J. Harding, J.P. Canales, and G.M. Kent. 2008. Upper crustal evolution along the Juan de Fuca Ridge flanks. *Geochemistry Geophysics Geosystems* 9, Q09006, http://dx.doi.org/10.1029/2008GC002085.

Nedimović, M.R., S.M. Carbotte, A.J. Harding, R.S. Detrick, J.P. Canales, J.B. Diebold, G.M. Kent, M. Tischer, and J.M. Babcock. 2005. Frozen magma lenses below the oceanic crust. *Nature* 436:1,149–1,152, http://dx.doi.org/10.1038/nature03944.

Newman, K., M.R. Nedimović, J.P. Canales, and S.M. Carbotte. 2011. Evolution of seismic Layer 2B at the Juan de Fuca Ridge from hydrophone streamer 2D traveltime tomography. *Geochemistry Geophysics Geosystems* 12, Q05009, http://dx.doi.org/10.1029/2010GC003462.

Perfit, M.R., D.J. Fonari, M.C. Smith, J.F. Bender, C.H. Langmuir, and R.M. Haymon. 1994. Small-scale spatial and temporal variations in mid-ocean ridge crest magmatic processes. *Geology* 22:375–379, http://dx.doi.org/10.1130/0091-7613(1994)022<0375:SSSATV>2.3.CO;2.

Perfit, M.R., V.D. Wanless, W.I. Ridley, E.M. Klein, M.C. Smith, A.R. Goss, J.S. Hinds, S.W. Kutza, and D.J. Fornari. 2012. Lava geochemistry as a probe into crustal formation at the East Pacific Rise. *Oceanography* 25(1):89–93, http://dx.doi.org/10.5670/oceanog.2012.06.

Rohr, K.M.M. 1994. Increase of seismic velocities in upper oceanic crust and hydrothermal circulation in the Juan de Fuca Plate. *Geophysical Research Letters* 19:2,163–2,166, http://dx.doi.org/10.1029/94GL01913.

Rohr, K.M.M., B. Milkereit, and C.J. Yorath. 1988. Asymmetric deep crustal structure across the Juan de Fuca Ridge. *Geology* 16:533–537, http://dx.doi.org/10.1130/0091-7613(1988)016<0533:ADCSAT>2.3.CO;2.

Rubin, K.H., J.D. Macdougall, and M.R. Perfit. 1994. ^{210}Po-^{210}Pb dating of recent volcanic eruptions on the sea floor. *Nature* 368:841–844, http://dx.doi.org/10.1038/368841a0.

Sims, K.W.W., J. Blichert-Toft, D.J. Fornari, M.R. Perfit, S.J. Goldstein, P. Johnson, D.J. DePaolo, S.R. Hart, M.T. Murrell, P.J. Michael, and others. 2003. Aberrant youth: Chemical and isotopic constraints on the origin of off-axis lavas from the East Pacific Rise, 9°–10°N. *Geochemistry, Geophysics, Geosystems* 4(10), 8621, http://dx.doi.org/10.1029/2002GC000443.

Singh, S.C., A.J. Harding, G.M. Kent, M.C. Sinha, V. Combier, S. Bazin, C.H. Tong, J.W. Pye, P.J. Barton, R.W. Hobbs, and others. 2006. Seismic reflection images of the Moho underlying melt sills at the East Pacific Rise. *Nature* 442:287–290, http://dx.doi.org/10.1038/nature04939.

Sinton, J.M., D.S. Wilson, D.M. Christie, R.N. Hey, and J.R. Delaney. 1983. Petrologic consequences of rift propagation on oceanic spreading ridges. *Earth and Planetary Science Letters* 62:193–207, http://dx.doi.org/10.1016/0012-821X(83)90083-3.

Soule, S.A., D.J. Fornari, M.R. Perfit, and K.H. Rubin. 2007. New insights into mid-ocean ridge volcanic processes from the 2005–2006 eruption of the East Pacific Rise, 9°46'N-9°56'N. *Geology* 35:1,079–1,082, http://dx.doi.org/10.1130/G23924A.1.

Tolstoy, M., J.P. Cowen, E.T. Baker, D.J. Fornari, K.H. Rubin, T.M. Shank, F. Waldhauser, D.R. Bohnenstiehl, D.W. Forsyth, R.C. Holmes, and others. 2006. A sea-floor spreading event captured by seismometers. *Science* 314:1,920–1,922, http://dx.doi.org/10.1126/science.1133950.

Toomey, D.R., E.E. Hooft, and W.S. Wilcock. 2010. Mantle flow beneath the Juan de Fuca and East Pacific Rise spreading centers and adjacent plates. *Eos, Transactions, American Geophysical Union* 90(52):Fall 2010 Meeting Abstract OS24A-03.

Toomey, D.R., D. Jousselin, R.A. Dunn, W.S.D. Wilcock, and R.S. Detrick. 2007. Skew of mantle upwelling beneath the East Pacific Rise governs segmentation. *Nature* 446:409–414, http://dx.doi.org/10.1038/nature05679.

Turner, S., C. Beier, Y. Niu, and C. Cook. 2011. U-Th-Ra disequilibria and the extent of off-axis volcanism across the East Pacific Rise at 9°30'N, 10°30'N, and 11°20'N. *Geochemistry Geophysics Geosystems* 12, Q0AC12, http://dx.doi.org/10.1029/2010GC003403.

Van Ark, E.M., R.S. Detrick, J.P. Canales, S. Carbotte, A.J. Harding, G.M. Kent, M.R. Nedimović, W.S.D. Wilcock, J.B. Diebold, and J.M. Babcock. 2007. Seismic structure of the Endeavour Segment Juan de Fuca Ridge: Correlations with seismicity, faulting and hydrothermal activity. *Journal of Geophysical Research* 112, B02401, http://dx.doi.org/10.1029/2005JB004210.

Vera, E.E., J.C. Mutter, P. Buhl, J.A. Orcutt, A.J. Harding, M.E. Kappus, R.S. Detrick, and T.M. Brocher. 1990. The structure of 0- to 0.2-m.y.-old oceanic crust at 9°N on the East Pacific Rise from expanded spread profiles. *Journal of Geophysical Research* 95(B10):15,529–15,556, http://dx.doi.org/10.1029/JB095iB10p15529.

Von Damm, K.L. 2004. Evolution of the hydrothermal system at East Pacific Rise 9°50'N: Geochemical evidence for changes in the upper oceanic crust. Pp. 285–304 in *Mid-Ocean Ridges: Hydrothermal Interactions Between the Lithosphere and Ocean*. C.R. German, ed., Geophysical Monograph 148, American Geophysical Union, Washington, DC.

Waters, C.L., K.W.W. Sims, M.R. Perfit, J. Blichert-Toft, and J. Blusztajn. 2011. Perspective on the genesis of E-MORB from chemical and isotopic heterogeneity at 9–10°N East Pacific Rise. *Journal of Petrology* 52(3):565–602, http://dx.doi.org/10.1093/petrology/egq091.

White, D.J., and R.M. Clowes. 1994. Seismic attenuation structure beneath the Juan de Fuca Ridge from tomographic inversion of amplitudes. *Journal of Geophysical Research* 99:3,043–3,056, http://dx.doi.org/10.1029/93JB02039.

Wilcock, W.S.D., and J.R. Delaney. 1996. Mid-ocean ridge sulfide deposits: Evidence for heat extraction from magma chambers or cracking fronts. *Earth and Planetary Science Letters* 145:49–64, http://dx.doi.org/10.1016/S0012-821X(96)00195-1.

Xu, M., J. Canales, H.D. Carton, S.M. Carbotte, M.R. Nedimović, and J.C. Mutter. 2010. 3D multi-channel seismic imaging of melt-rich lenses beneath and off the East Pacific Rise Integrated Study Site. *Eos, Transactions, American Geophysical Union* 90(52):Fall Meeting Abstract OS21C-1513.

Zha, Y., S.L. Nooner, W.C. Crawford, and S.C. Webb. 2010. Modeling of 3D crustal shear structures from compliance measurements near East Pacific Rise 9°50'. *Eos, Transactions, American Geophysical Union* 90(52):Fall Meeting Supplement Abstract OS21C-1509.

Zou, H., A. Zindler, and Y. Niu. 2002. Constraints on melt movement beneath the East Pacific Rise from ^{230}Th–^{238}U disequilibrium. *Science* 295:107–110, http://dx.doi.org/10.1126/science.1064295.